

# Proximity-induced magnetization and towards the efficient spin gating in graphene

Mihovil Bosnar,<sup>1,\*</sup> Ivor Lončarić,<sup>1,†</sup> P. Lazić,<sup>2,1</sup> K. D. Belashchenko,<sup>3</sup> and Igor Žutić<sup>4</sup>

<sup>1</sup>*Ruder Bošković Institute, 10000 Zagreb, Croatia*

<sup>2</sup>*Research Computing Support Services group, University of Missouri, Columbia, MO, 65211-7010, USA*

<sup>3</sup>*University of Nebraska-Lincoln and Nebraska Center for Materials and Nanoscience, Lincoln, NE 68588-0299, USA*

<sup>4</sup>*University at Buffalo, State University of New York, Buffalo, NY 14260-1500, USA*

Instead of the commonly used chemical doping, it can be more favorable to consider transforming graphene through proximity effects by carefully choosing its adjacent regions. While gate-tunable room-temperature spin-dependent properties could be induced in graphene by magnetic proximity effects from common metallic ferromagnets, this approach is complicated by chemical bonding between a metal and graphene suggesting the need for an intervening buffer layer. However, even with a buffer layer there is still a large energy shift of the Dirac cone in graphene away from the Fermi level. Compared to such a large negative shift and its resulting  $n$ -doping when graphene is separated from cobalt by a monolayer h-BN or another layer of graphene, we show that it can be favorable to instead separate graphene by a monolayer of gold or platinum. The resulting proximity induced magnetization is larger, energy shift is somewhat reduced and changes its sign, offering a path for proximity-induced spin polarization in graphene which can be tuned at smaller gate-controlled electric field than for the h-BN buffer layer.

## I. INTRODUCTION

Despite its attractive properties, there is a strong interest to modify graphene (Gr) by introducing superconductivity, magnetism, a sizeable energy gap, or strong spin-orbit coupling. A common approach to accomplish this by chemical doping or functionalization typically poses inherent difficulties, from introducing unwanted disorder to significantly reducing Gr's high mobility [1]. An alternative approach to transform graphene and overcome these difficulties is provided by proximity effects, whereby it acquires properties of its neighbors, for example, becoming superconducting, magnetic, topologically nontrivial, or with an enhanced spin-orbit coupling [2–8]. Being atomically thin, Gr and a growing class of two-dimensional (2D) materials are changed significantly even with short-range proximity effects [1].

In this work we focus on magnetic-proximity effects in Co/Gr-based heterostructures, as shown in Fig. 1, that could enhance spintronic applications. However, the interest in magnetic-proximity effects in 2D systems is much broader, as they are considered for implementing magnetic skyrmions [9] and exotic properties of topological insulators [10], as well as realizing Majorana bound states for topological quantum computing [11–14].

With its high mobility and low spin-orbit coupling, Gr is expected to be a particularly suitable material for spin transport and spintronics [15–17]. From the first demonstration of spin injection in Gr [18], there was a significant progress in extending characteristic timescales and lengthscales over which the spin information can be sustained [19, 20]. Gr-based spin-logic gates have been demonstrated at room temperature [21], supporting pro-

posals for specialized applications which could outperform CMOS-based counterparts [22].

Many spintronic applications rely on ferromagnet(F)/Gr junctions as their building block where the functionalities are realized by changing the magnetization orientation in multiple ferromagnetic layers [15–17, 23–25]. An alternative approach, to those employing an external applied magnetic field, is to take advantage of the electrically-tunable magnetic proximity effect in Gr, which is potentially faster and more energy-efficient [26, 27]. Both the magnitude and the sign of proximity-induced spin polarization in Gr can be controlled by electric gating [26].

Common expectations for tunable magnetic proximity effects imply that magnetic insulator is required to avoid a short-circuit effect of a metallic F [28–33]. This is further supported since Gr forms a strong chemical bonding on Co [26, 34, 35] which removes its spin degeneracy, but also essentially turns Gr into a metallic continuation of Co with a large density of states (DOS) near the Fermi level. Because of that, it is practically impossible to change the spin polarization of Gr on Co by applying the gate electric field [26].

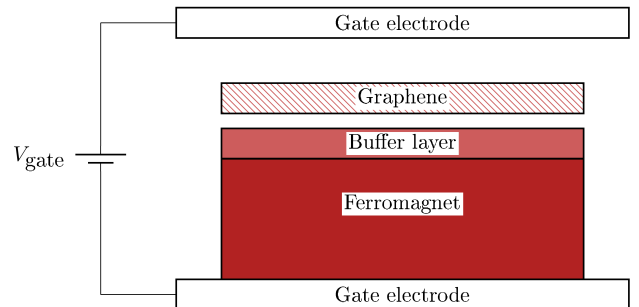


FIG. 1. Schematic view of the system.

\* mbosnar@irb.hr

† ivor.loncaric@gmail.com

Therefore, the idea to select heterostructures with a van der Waals (vdW) bonded layer of Gr was introduced [26]. A common metallic F with high Curie temperature could then be considered for tunable magnetic proximity effects. In particular, surface passivation through an addition of another Gr layer [26] or a layer of h-BN [26, 34] as a buffer between Gr and Co, as shown in Fig. 1, was studied. In both cases the passivation results in the top layer of Gr being bound to the underlying structure by the vdW interaction [26].

A characteristic property of vdW bonding is that it preserves the features of the electronic structure of bound systems, such as the Dirac cone in Gr [26, 35, 36]. However, a few major differences in comparison to a free-standing system are also introduced. In systems studied previously, the most relevant are the (*n*-type) doping [26, 35] and removing the spin degeneracy due to the proximity effect [26, 34]. The change in the electronic states near the Fermi level compared to the free-standing Gr can be described as a spin-dependent band shift [26]. This is supported by the recent transport experiments [36]. The role of Gr was not viewed as a spin filter [37], but a source of spin-polarized carriers itself, arising from an interplay of doping by the metallic F and the proximity-induced spin splitting in graphene [36].

Gr and the passivated surface can be thought of as two plates of a capacitor; gate voltage produces an electrostatic potential difference and charge transfer between them. This changes the spin polarization of Gr at the Fermi level in magnitude and sometimes even sign [26, 34]. An electrostatic model based on this picture predicts that the induced potential difference between the slab and Gr is increased by lowering the DOS at the Fermi level in graphene [26]. It is, therefore, expected that the spin polarization should be more sensitive to gating if the Fermi level is close to the Dirac point in Gr.

With previously studied h-BN and Gr passivation layers, it was found that the physisorbed Gr is *n*-doped and the apex of its Dirac cone is shifted approximately 0.5 eV below the Fermi level, resulting in relatively large DOS at the Fermi level [26]. First-principles calculations have shown that tuning the DOS spin polarization in Gr in this system requires large electric fields [26], achievable only by liquid gating [38, 39] and unsuitable for applications. This is further corroborated experimentally in lateral Co/h-BN/Gr-based spin valves [40]. Within the 2D ferromagnetic contacts in a planar geometry, similar as that depicted in Fig. 1, an electrostatic gating failed to produce tunable magnetic proximity effects. Instead, to reduce a detrimental *n*-doping of Gr, 1D edge contacts were used to realize such gate-controlled tunability and the reversal of proximity-induced spin polarization in Gr [40].

In this work we explore a path to reduce the magnitude of electric fields and realize tunable spin polarization in common 2D geometries by recognizing that Gr on Au and Pt is predicted to have *p*-doping [35] and could partially counteract the *n*-doping of Co contacts. Our

related first-principles calculations provide guidance towards optimized structures for proximity-induced magnetization and spin gating in Gr, which allows spin control of its electronics properties. While the two doping effects are not cancelled, compared to Co/h-BN/Gr heterostructures Au or Pt passivation yields more than an order of magnitude larger spin polarization in Gr at electric fields  $< 0.01$  V/Å, within the range of electrostatic gating, reaching 15 % with Pt.

## II. COMPUTATIONAL DETAILS

Proximity-induced spin polarization of graphene was studied using density functional theory (DFT) as implemented in a real-space code GPAW [42–44]. The reason for using a real space approach instead of a plane wave expansion is to avoid the use of periodic boundary conditions in the non-periodic direction of the system to prevent electron tunneling in that direction [26], since such use of the periodic boundary conditions introduces spurious interactions with periodically repeated images of the system which need to be corrected [45].

In all calculations the semilocal vdW exchange-correlation functional vdw-df-cx [46–48] from the libvdwxc library [49] was used. The cell was sampled by a grid of 0.1332 Å spacing in the planes parallel to the heterostructure layers, and 0.166 Å in the perpendicular direction. The GPAW PAW [50, 51] PBE [52] setups were used for all calculations.

Input structures were constructed in QuantumWise Virtual NanoLab [53]. The slab of hexagonal close-packed Co terminated by a (0001) surface was modeled by 7 layers of atoms. The passivating Au and Pt monolayers were added in an extension of this slab, forming a  $1 \times 1$  supercell. Since the lattice constant of Gr ( $a = 2.46$  Å) is similar to that of the Co (0001) surface ( $a = 2.51$  Å), the slab was strained 2.3 % so that it forms a  $1 \times 1$  supercell with Gr, which greatly reduces the computational burden compared to working with larger supercells. The cell contained 10 Å of vacuum on both sides of the heterostructure.

Since Gr can be positioned differently relative to the surface atoms, the systems were first relaxed in three high-symmetry configurations (Au or Pt atom located above the hollow site of Gr, over a bond between the two C atoms in the unit cell, or on top of one of them) to find the one with the lowest energy. The relaxations were done using the BFGS line search (Quasi Newton) algorithm as implemented in the ASE package [44], with GPAW as the DFT calculator. The relaxations were performed until the force between the atoms was smaller than 0.05 eV/Å, with a  $15 \times 15 \times 1$  Monkhorst-Pack sampling of the Brillouin zone, the Fermi-Dirac smearing of 200 meV and the bottom two layers of Co fixed.

The calculations show that the configuration in which the Au/Pt atoms are located above the hollow sites of Gr, shown in Fig. 2, is optimal for both passivation layers.

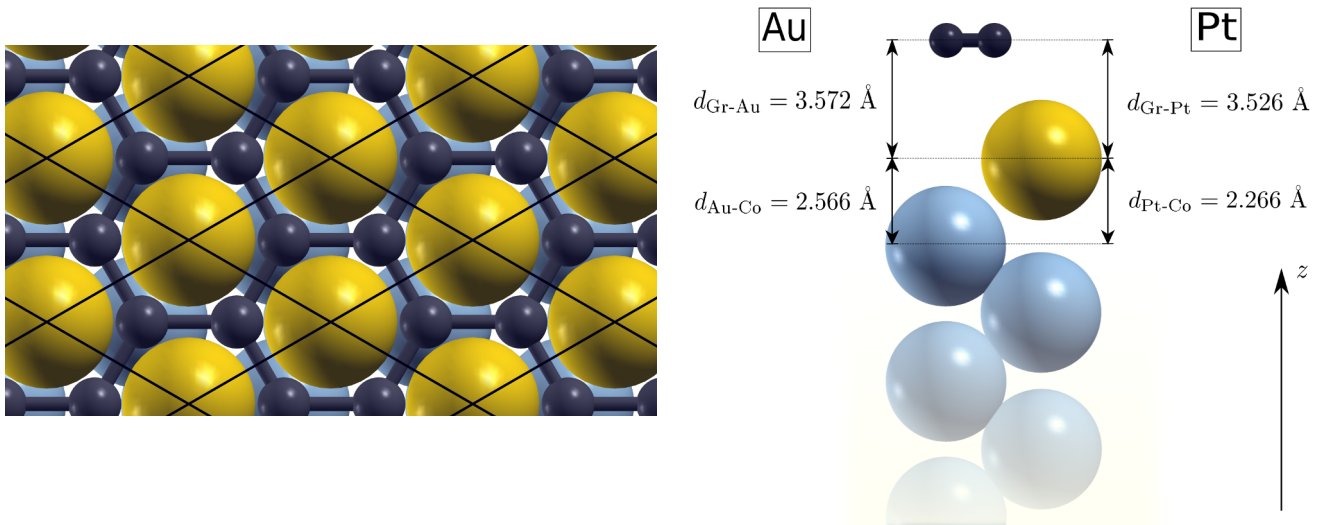


FIG. 2. Top (left) and side (right) view of the optimal energy structure. C atoms are shown in dark blue, noble metal in yellow and Co in light blue. The interlayer distances correspond to the equilibrium without the applied field. Figure was made using the XCrySDen software [41].

The obtained optimal Co/Au/Gr and Co/Pt/Gr structures were relaxed further with a homogeneous electric field included in the  $\pm z$  direction. The field magnitudes of  $0.01 \text{ V/\AA}$ ,  $0.05 \text{ V/\AA}$ ,  $0.1 \text{ V/\AA}$  and  $0.2 \text{ V/\AA}$  were used. To improve the precision of the calculated magnetic moments, a self-consistent calculation was performed for each relaxed structure with a dense  $63 \times 63 \times 1$  k-point mesh and the Fermi-Dirac smearing of 10 meV. The magnetic moments are estimated as a projection of the spin density

$$\mathcal{M}(\mathbf{r}) = \rho_{\uparrow}(\mathbf{r}) - \rho_{\downarrow}(\mathbf{r}), \quad (1)$$

on the localized atomic setup functions.

A large number of  $k$  points is also needed to resolve the Dirac cone of Gr in the calculations of the projected density of states (PDOS) on carbon atoms. The PDOS was calculated with the Gaussian broadening of 200 meV.

The STM images were simulated following the Tersoff-Hamann theory [54], as implemented in the ASE package. The ASE tool was modified so that the images can be made separately for the two spin channels.

### III. RESULTS AND DISCUSSION

#### III.1. Zero-gate voltage

The band structures of both systems without the applied field are shown in Fig. 3. Clearly, in both cases the Dirac cone of Gr is preserved upon adsorption but shifted to higher energies by approximately 0.369 eV and 0.295 eV in the case of Pt and Au passivation layer, respectively. Along with the obtained distances of about

$3.5 \text{ \AA}$  between Gr and the Pt or Au layer (Fig. 2), these results suggest vdW bonding between Gr and the metal. Gr is p-doped by an amount somewhat smaller than the  $n$ -doping of Gr in the system with a h-BN passivation layer [26]. As shown in the insets in Fig. 3, lifting of the spin degeneracy is also induced in Gr.

According to the model Hamiltonian of Gr in contact with passivated Co surfaces [34], the spin splitting can be separated into two contributions: Exchange splitting that is constant in energy and  $k$  near the Fermi level and  $K$  point, and the energy and  $k$  dependent contribution due to hybridization. The exchange part can be estimated as a difference of the energies of spin-up and spin-down Gr bands far away from the avoided crossings, while the hybridization contribution is more difficult to quantify.

The spin splitting of the Gr bands in Co/Au/Gr is approximately constant near the Fermi level, as illustrated in the inset of Fig. 3(a), and averages to about 1.05 meV. In contrast, the gaps at the avoided crossings, such as the one shown in Fig. 3(b), are so large in Co/Pt/Gr that the spin splitting is not uniform in any part of the band structure near the Fermi level.

The larger spin splitting on avoided crossings for Pt passivation layer can be understood from the orbital analysis of the flat band near the Fermi level, which shows that this band have dominantly contributions from the orbitals of Pt and the first Co layer under it. For the Au passivation layer the flat bands contributions does not come from Co atoms close to surface or Au orbitals, but from bulk Co atoms.

This is because the spin-down  $d$  states of both Pt and Co are partially filled and can be found near the Fermi level, which in turn allows their strong hybridization in forming of the chemical bond between Pt and Co. Additionally, Pt is close to fulfilling the Stoner criterion,

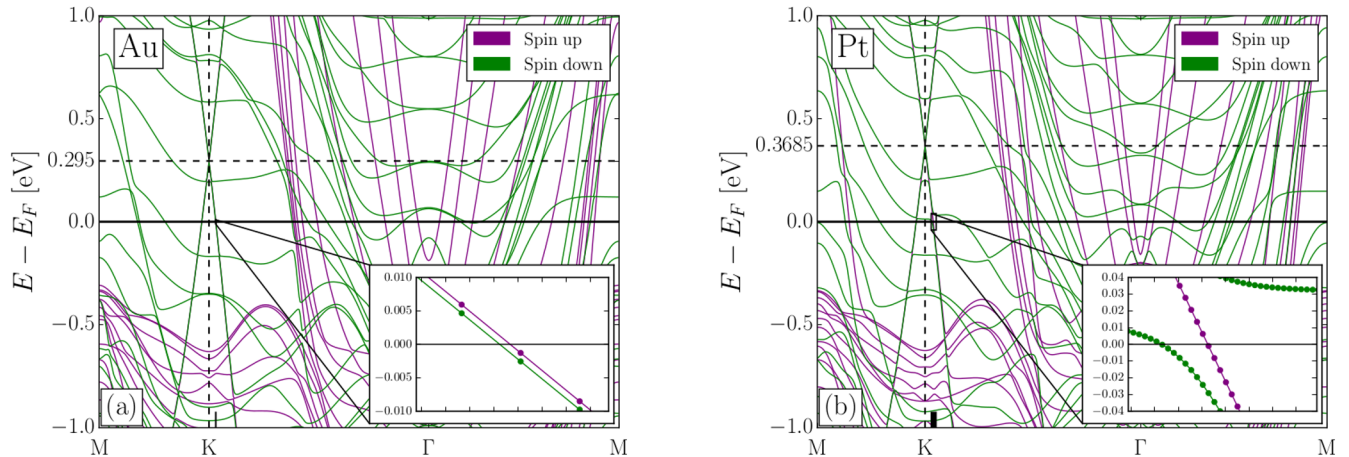


FIG. 3. The band structure of (a) Co/Au/Gr and (b) Co/Pt/Gr. Insets: enlarged portion of the band structure near the Fermi level. The width of the black rectangles on the  $x$  axis denotes width of the enlarged area. Note the different scales on insets.

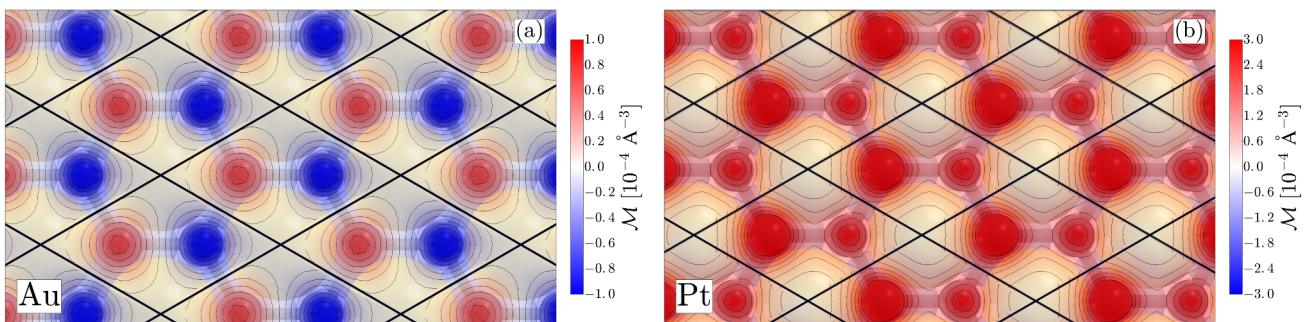


FIG. 4. Spin density in (a) Co/Au/Gr and (b) Co/Pt/Gr in a plane  $0.33 \text{ \AA}$  above the graphene layer. Red (blue) areas: same (opposite) sign of the spin density as in Co. Note the different scale of the colorbars. Figure was made using the XCrySDen software [41].

meaning the electron correlations are strong enough to cause significant spin splitting of hybrid states. On the other hand, the  $d$  states of Au are fully occupied so its  $d$  states are located far from the Fermi level.

Therefore, polarized surface bands are present on Pt in the Co/Pt/Gr system, which means their overlap with Gr orbitals is larger than in the case of polarized bands of Co/Au/Gr, and the larger spin degeneracy splitting is induced in Gr.

As a result of the spin splitting there is a finite spin density in Gr. The magnetization of graphene in Co/Au/Gr can be estimated from the Pauli susceptibility of pristine graphene. On one hand, it can be obtained by subtracting the integrals of spin-up and spin-down PDOS in graphene over the filled states, which gives  $-9.27 \times 10^{-6} \mu_B$ . On the other hand, calculating it from the Pauli susceptibility, with the exchange field playing role of magnetic field, gives  $-8.61 \times 10^{-6} \mu_B$  (note that positive splitting as defined above yields spin-down polarization of graphene as spin-up band is raised in energy compared to spin-down). Similar prediction cannot be

made for Co/Pt/Gr.

However, the spin density of graphene is not homogeneous in either system because surface is not homogeneous. The plot of the spin density plane cut at  $0.33 \text{ \AA}$  above the graphene in Fig. 4 shows that in the case of Co/Pt/Gr only the magnitude of the induced spin density in graphene varies, while in Co/Au/Gr the sign varies as well.

Spin-dependent transport effects are sensitive to the spin polarization  $P(E)$  of the PDOS  $N_s(E)$  as

$$P(E) = \frac{N_{\uparrow}(E) - N_{\downarrow}(E)}{N_{\uparrow}(E) + N_{\downarrow}(E)}, \quad (2)$$

which, near the the Fermi level, is smaller in Co/Au/Gr compared to Co/Pt/Gr, as can be seen from Figs 5(a) and (b). This is not caused by the variation of the sign of the spin density in space as seen in Fig. 4. By integrating the PDOS per atom  $a$  in a selected spin channel in an

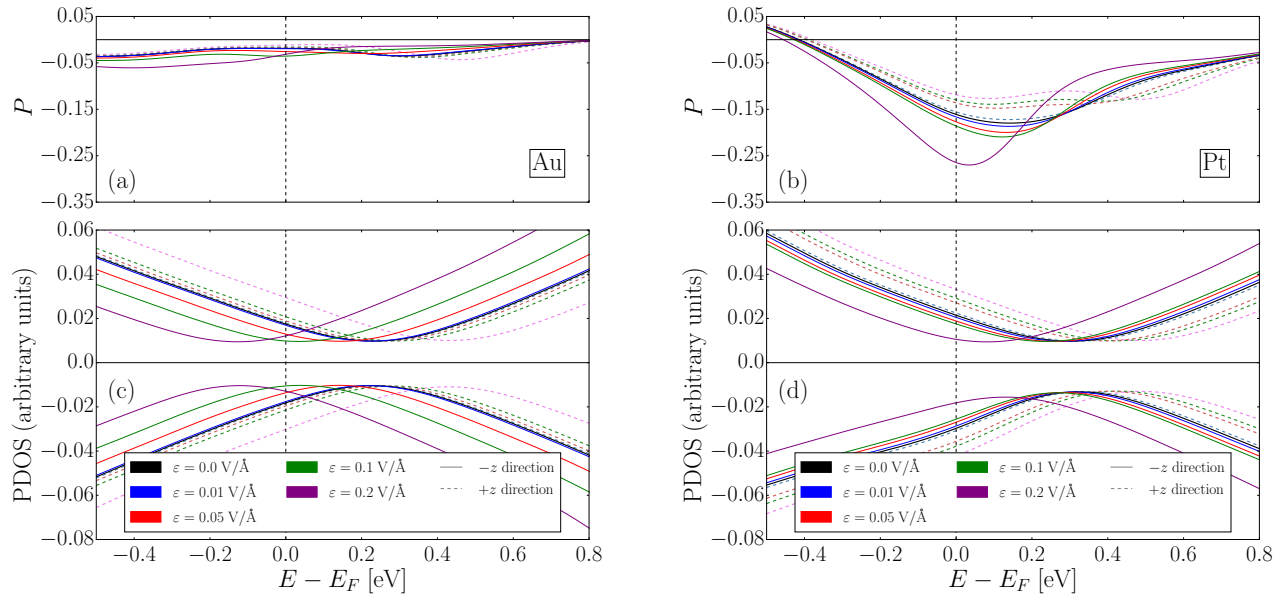


FIG. 5. (a-b) energy-resolved spin polarization [Eq. (2)] and (c-d) PDOS in graphene in Co/Au/Gr [panels (a) and (c)] and Co/Pt/Gr [panels (b) and (d)].  $N_{\downarrow}(E)$  is plotted with negative sign. Colored solid (dashed) lines: PDOS with field directed from Gr to the metal (from the metal to Gr). The vertical dashed line denotes the Fermi level. The PDOS does not reach zero as expected, because of the broadening used in calculations.

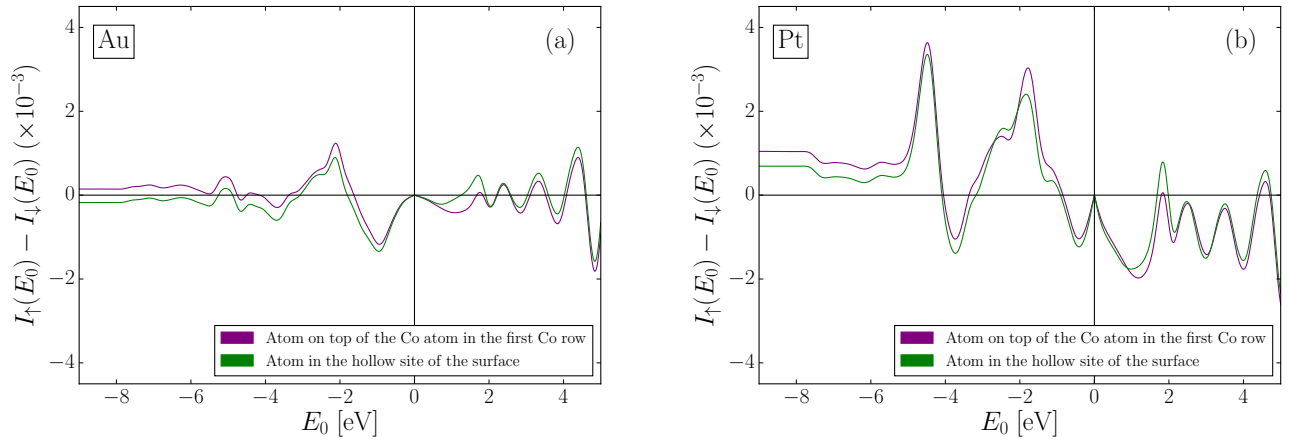


FIG. 6. The difference of integrals [Eq. 3] of the atomic PDOS from the Fermi level to some selected energy  $E_0$  between the two spin channels, in dependence to this energy.

interval from the Fermi level to a selected energy  $E_0$

$$I_s^a(E_0) = \text{sgn}(E_F - E_0) \int_{E_0}^{E_F} N_{a,s}(E) dE, \quad (3)$$

and subtracting the results for the spin channels, the contribution of the bands in the selected energy range to the atomic spin density is obtained. From the dependence of this difference on the selected  $E_0$  for graphene, shown in Fig. 6, it is clear that near the Fermi level the  $\pi$  bands give a "ferromagnetic" contribution to the net polarization in case of both Au and Pt passivation layer.

Therefore, the spin polarization of graphene  $\pi$  bands

near the Fermi level is larger for Co/Pt/Gr than for Co/Au/Gr only because of a much larger spin splitting in graphene near the Fermi level in former compared to latter, as discussed previously. Particularly, in the case of the Pt passivation layer, there is a surface band in the spin down channel around 12 meV above the Fermi level, which causes large splitting on the avoided crossing. Such a band is absent in the case of Co/Au/Gr.

Furthermore, Fig. 6 also shows that regardless of the passivation layer, the contributions of graphene bands up to 8 eV below the Fermi level have to be included in order to obtain the spin density shown in Fig. 4. This

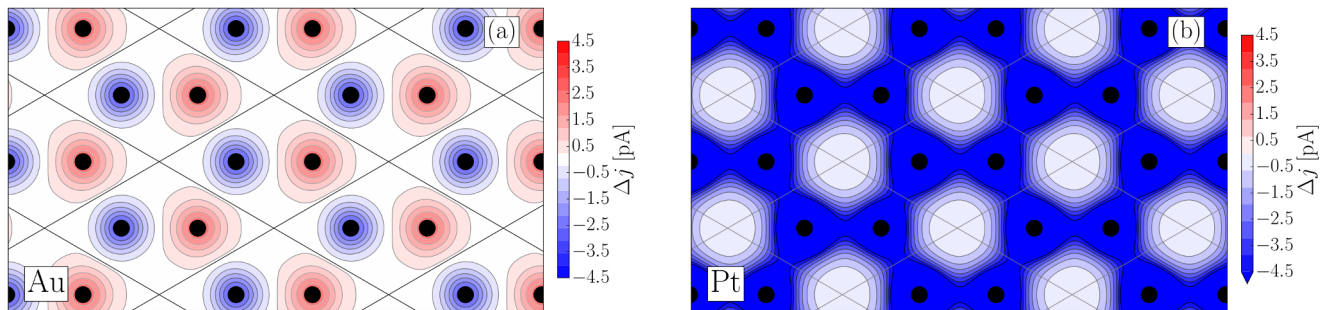


FIG. 7. The difference between the simulated STM currents in two spin channels at a constant height of  $1 \text{ \AA}$  above Gr and the positive bias of  $1.5 \text{ V}$  (i. e. a scan of the empty states) for the system with the Au (left) and Pt (right) passivation layers. Black circles denote the positions of C atoms.

means that not only the  $\pi$  bands of graphene are spin polarized by the proximity effect, but also a part of its  $\sigma$  bands. The energy range in which the graphene orbitals are spin polarized corresponds to the range of energies of the  $d$  bands of the metals. Hence, we conclude that the hybridization of graphene bands with the  $d$  bands of the metal gives rise to the proximity effect. We note that the total spin density differs significantly from the Fermi level spin density. This is because hybridization caused by avoided crossings far from the Fermi level also brings about additional charge transfer.

The energy-dependent spin-polarized DOS in Gr could be measured experimentally by a spin-polarized STM. According to Fig. 6, by selecting an appropriate bias a varying sign or a constant sign image could be seen in either system. In Fig. 7 we show an example of the difference of the simulated spin-resolved STM images, where the bias of the STM was selected so that the net spin polarization of the scanned orbitals in the system with the Au passivation layer varies in sign. For the same bias, the simulated difference in the system with the Pt passivation layer is constant in sign.

### III.2. Effects of gating

With the gate electric field applied, charge is transferred between the metal and Gr. This produces a shift of the PDOS relative to the Fermi level, as shown in Figs. 5(c) and (d). The shift can be traced through the position of the point where the PDOS has a minimum. This point moves away from the Fermi level for fields oriented along the positive  $z$  direction because the electronic states of Gr are raised in energy compared to the metal and electrons flow from Gr to the metal, and vice versa.

For the same magnitude of the electric field, the PDOS of the system with the Au passivation layer shifts more than the PDOS of the system with the Pt passivation layer. This is in agreement with the electrostatic

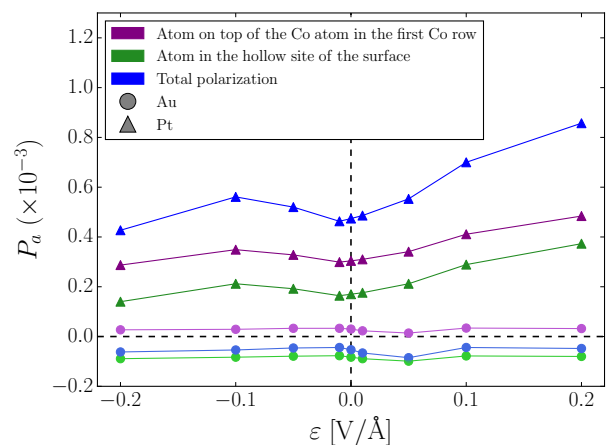


FIG. 8. Comparison of the atomic magnetic moments of C atoms of Gr for the system with Au (circles, lighter shade) and Pt (triangles, darker shade) passivation layer. Lines are guide to the eye.

model [26], as the doping of Gr for the Au passivation layer is lower, and consequently the PDOS at the Fermi level is smaller compared to Pt.

However, the change in the spin density does not directly reflect the amount of the charge transferred. Figure 8 shows the magnetic moments of C atoms of Gr as a function of the gate field magnitude. It is clear that the field-induced change in magnetic moments is greater in the case of the Pt passivation layer. Furthermore, the spin polarization of bands near the Fermi level as a function of the magnitude of the gate field is shown in Fig. 5(a) and (b). Similarly to the magnetic moments, the energy-resolved spin polarization for the system with the Au passivation layer is less responsive to the gate field.

Stronger response in Co/Pt/Gr is due to the presence of spin-polarized bands with strong surface character slightly above the Fermi level. An electric field

applied in the positive  $z$  direction lifts the surface bands higher above the Fermi level, because they are localized on the side of the metal with lower electrostatic potential, and vice versa. Due to the strong dispersion near the avoided crossing in the spin-down channel, this shift results in a significant change in the polarization when the electric field is applied.

For Co/Au/Gr the surface character of  $d$  bands is less pronounced and these bands shift significantly less with the applied field. On the other hand, the homogeneous splitting caused by interlayer exchange is unaffected by the field. Therefore, the total change in polarization of Gr in Co/Au/Gr is significantly smaller than in Co/Pt/Gr.

The previously studied system with a h-BN passivation layer also exhibits a change in the sign of the spin polarization at the Fermi level with large gate field [26, 34]. Due to different electronic configuration in Co/Pt/Gr or Co/Au/Gr, the sign of the spin polarization at the Fermi level does not change with the tested gate fields.

#### IV. CONCLUSIONS

We have studied a system consisting of the ferromagnetic Co slab passivated by a layer of Au or Pt and a physisorbed layer of graphene which develops spin polarization through the proximity effect. This polarization can be tuned by the electric field, similarly to the previously studied systems where h-BN or graphene were used as passivation layers [26, 34]. Another manifestation of the magnetic proximity is the induced spin density in the graphene layer, which has the same (opposite) sign on the two inequivalent carbon atoms in Co/Pt/Gr (Co/Au/Gr). The net polarization is produced by the polarization of both  $\sigma$  and  $\pi$  orbitals in the energy range where the  $d$  bands of the metal are found. Inequivalence of induced polarization of carbon atoms manifests through different spin resolved local density of states on these carbon atoms which can be experimentally tested with a spin-polarized STM [55].

For spintronic applications relying on transport [55], the spin polarization near the Fermi level is important. Graphene in the Co/Pt/Gr system shows larger polarization near the Fermi level and stronger response to the applied field compared to Co/Au/Gr. Without an applied electric field, the spin polarization for both passivation layers is larger compared to the previously studied Co/h-BN/Gr system [26], while the response to the electric field is only slightly stronger.

The large Gr spin polarization at the Fermi level in Co/Pt/Gr originates from the presence of a spin-down surface band just above the Fermi level. Stronger response to the electric field in this system is mediated by the field-induced shift of this band and is also facilitated by the lower doping of graphene compared to the systems with h-BN or Gr passivation layers. However, because

the response to the field is weaker in Co/Au/Gr where the doping level is even lower compared to Co/Pt/Gr, we conclude that the effect of the surface band is the most important.

While Co/Au/Gr and Co/Pt/Gr do not exhibit gate-controlled reversal of the proximity-induced spin polarization, which could be useful for implementation of Gr-based magnetologic gates and lateral spin-valves [15, 16, 21, 40], we have obtained several important findings, discussed below, which could also stimulate future work. Co/Pt/Gr-based structures support gate-controlled modulation of spin polarization, which is the key element of spin-interconnects [1]. Their constant-level charge current eliminates the crosstalk problems of unintended signals from electromagnetic induction in the neighboring wires based on the modulation of charge current in conventional interconnects [56].

Since Au and Pt layers are spatially closer to Gr than Co, their  $p$ -doping character dominates the position of the Dirac cone compared to the  $n$ -doping of Gr by Co known from Co/h-BN/Gr heterostructures [26, 34, 36]. Further studies should concentrate on finding the surfaces where doping is lower, by changing Au and Pt layer concentration and their different spatial positions, as well as the surfaces that feature polarized surface bands on the Fermi level.

Elucidating magnetic proximity effects in graphene heterostructures with metallic ferromagnets remains an important issue as recent experiments on bias-dependent reversal of magnetoresistance in vertical Co/Gr/NiFe spin valves support an overlooked role of graphene [36]. Instead of ideally lattice-matched single-crystalline ferromagnet/Gr structures required for effective spin filtering [37], they confirm the formation of van der Waals heterostructures without such lattice matching where the proximitized graphene itself is a source of spin-polarized carriers [26, 36]. While in these experiments Co and NiFe were responsible for effective  $n$ - and  $p$ -doping of graphene [36], our studies show that even with a single ferromagnet, both  $n$ - and  $p$ -doping of graphene is possible, which could enable different approaches for designing bias-dependent magnetoresistive effects [25, 36, 57, 58].

#### ACKNOWLEDGMENTS

M.B. and I.L. acknowledge support from Croatian Science Foundation and the European Union through the European Regional Development Fund within the Competitiveness and Cohesion Operational Programme (Grant No. KK.01.1.1.06). K.D.B. is supported by NSF through Grant No. DMR-1609776 and the Nebraska Materials Research Science and Engineering Center (MRSEC) Grant No. DMR-1420645. I.Z. acknowledges support from US ONR N000141712793 and NSF ECCS-1810266, US ONR N000141712793, and UB Center for Computational Research.

- 
- [1] I. Žutić, A. Matos-Abiague, B. Scharf, H. Dery, and K. Belashchenko, “Proximitized materials,” *Mater. Today* **22**, 85 (2019).
- [2] H. B. Heersche, P. Jarillo-Herrero, J. B. Oostinga, L. M. K. Vandersypen, and A. F. Morpurgo, “Bipolar supercurrent in graphene,” *Nature* **446**, 56 (2007).
- [3] P. Wei, S. Lee, F. Lemaître, L. Pinel, D. Cutaia, W. Cha, F. Katmis, Y. Zhu, D. Heiman, J. Hone, J. S. Moodera, and C.-T. Chen, “Strong interfacial exchange field in the graphene/EuS heterostructure,” *Nat. Mater.* **15**, 711 (2016).
- [4] M. Gmitra, D. Kochan, P. Högl, and J. Fabian, “Trivial and inverted Dirac bands and emergence of quantum spin Hall states in graphene on transition-metal dichalcogenides,” *Phys. Rev. B* **93**, 155104 (2016).
- [5] A. Avsar, J. Y. Tan, T. Taychatanapat, J. Balakrishnan, G. K. W. Koon, Y. Yeo, J. Lahiri, A. Carvalho, A. S. Rodin, E. C. T. O’Farrell, G. Eda, A. H. Castro Neto, and B. Özyilmaz, “Spin-orbit proximity effect in graphene,” *Nat. Commun.* **5**, 4875 (2014).
- [6] E. Rossi and C. Triola, “van der Waals heterostructures with spin-orbit coupling,” *Ann. Phys.* **in press** (2020).
- [7] J. Lee and J. Fabian, “Magnetotransport signatures of the proximity exchange and spin-orbit couplings in graphene,” *Phys. Rev. B* **94**, 195401 (2016).
- [8] J.-B. Qiao, Y. Gong, H. Liu, J.-A. Shi, L. Gu, and L. He, “Two-dimensional spinodal interface in one-step grown graphene-molybdenum carbide heterostructures,” *Phys. Rev. Materials* **2**, 054002 (2018).
- [9] H. Yang, G. Chen, A. A. Cotta, A. T. N’Diaye, S. A. Nikolaev, E. A. Soares, W. A. A. Macedo, A. K. Schmid, A. Fert, and M. Chshiev, “Significant Dzyaloshinskii-Moriya interaction at graphene-ferromagnet interfaces due to Rashba-effect,” *Nat. Mater.* **17**, 605 (2018).
- [10] X.-L. Qi and S.-C. Zhang, “Topological insulators and superconductors,” *Rev. Mod. Phys.* **83**, 1057 (2011).
- [11] J. Sau, R. M. Lutchyn, S. Tewari, and S. D. Sarma, “Generic new platform for topological quantum computation using semiconductor heterostructures,” *Phys. Rev. Lett.* **104**, 040502 (2010).
- [12] G. L. Fatim, A. Matos-Abiague, B. Scharf, and I. Žutić, “Wireless Majorana bound states: From magnetic tunability to braiding,” *Phys. Rev. Lett.* **117**, 077002 (2016).
- [13] T. Zhou, N. Mohanta, J. E. Han, A. Matos-Abiague, and I. Žutić, “Tunable magnetic textures in spin valves: From spintronics to Majorana bound states,” *Phys. Rev. B* **99**, 134505 (2019).
- [14] M. M. Desjardins, L. C. Contamin, M. R. Delbecq, M. C. Dartiailh, L. E. Bruhat, T. Cubaynes, J. J. Viennot, F. Mallet, S. Rohart, A. Thiaville, A. Cottet, and T. Kontos, “Synthetic spin-orbit interaction for Majorana devices,” *Nat. Mater.* **18**, 1060 (2019).
- [15] W. Han, R. K. Kawakami, M. Gmitra, and J. Fabian, “Graphene spintronics,” *Nat. Nanotechnol.* **9**, 794 (2014).
- [16] X. Lin, W. Yang, K. L. Wang, and W. Zhao, “Two-dimensional spintronics for low-power electronics,” *Nat. Electron.* **2**, 274 (2019).
- [17] A. Avsar, H. Ochoa, F. Guinea, B. Özyilmaz, B. J. van Wees, and I. J. Vera-Marun, “Colloquium: Spintronics in graphene and other two-dimensional materials,” *Rev. Mod. Phys.* **in press** (2020).
- [18] N. Tombros, C. Józsa, M. Popinciuc, H. T. Jonkman, and B. J. van Wees, “Electronic spin transport and spin precession in single graphene layers at room temperature,” *Nature* **448**, 571 (2007).
- [19] M. Drögeler, F. Volmer, M. Wolter, B. Terrés, K. Watanabe, T. Taniguchi, G. Güntherodt, C. Stampfer, and B. Beschoten, “Nanosecond spin lifetimes in single- and few-layer graphene-hBN heterostructures at room temperature,” *Nano Lett.* **14**, 6050 (2014).
- [20] P. J. Zomer, M. H. D. Guimarães, N. Tombros, and B. J. van Wees, “Long-distance spin transport in high-mobility graphene on hexagonal boron nitride,” *Phys. Rev. B* **86**, 161416(R) (2012).
- [21] H. Wen, H. Dery, W. Amamou, T. Zhu, Z. Lin, J. Shi, I. Žutić, I. Krivorotov, L. J. Sham, and R. K. Kawakami, “Experimental demonstration of XOR operation in graphene magnetologic gates at room temperature,” *Phys. Rev. Appl.* **5**, 044003 (2016).
- [22] H. Dery, H. Wu, B. Ciftcioglu, M. Huang, Y. Song, R. K. Kawakami, J. Shi, I. Krivorotov, I. Žutić, and L. J. Sham, “Nanospintronics based on magnetologic gates,” *IEEE Trans. Electron. Dev.* **59**, 259 (2012).
- [23] P. Lazić, G. M. Sipahi, R. K. Kawakami, and I. Žutić, “Graphene spintronics: Spin injection and proximity effects from first principles,” *Phys. Rev. B* **90**, 085429 (2014).
- [24] B. Raes, A. W. Cummings, F. Bonell, M. V. Costache, J. F. Sierra, S. Roche, and S. O. Valenzuela, “Spin precession in anisotropic media,” *Phys. Rev. B* **95**, 085403 (2017).
- [25] S. Ringer, M. Rosenauer, T. Völkl, M. Kadur, F. Hopperditzel, D. Weiss, and J. Eromsa, “Spin field-effect transistor action via tunable polarization of the spin injection in a Co/MgO/graphene contact,” *Appl. Phys. Lett.* **113**, 132403 (2018).
- [26] P. Lazić, K. D. Belashchenko, and I. Žutić, “Effective gating and tunable magnetic proximity effects in two-dimensional heterostructures,” *Phys. Rev. B* **93**, 241401(R) (2016).
- [27] B. Zhao, D. Khokhriakov, B. Karpiak, A. M. Hoque, L. Xu, L. Shen, Y. P. Fen, X. Xul, Y. Jiang, and S. P. Dash, “Electrically controlled spin-switch and evolution of Hanle spin precession in graphene,” *2D Mater.* **6**, 035042 (2019).
- [28] H. X. Yang, A. Hallal, D. Terrade, X. Waintal, S. Roche, and M. Chshiev, “Proximity effects induced in graphene by magnetic insulators: First-principles calculations on spin filtering and exchange-splitting gaps,” *Phys. Rev. Lett.* **110**, 046603 (2013).
- [29] Z. Wang, C. Tang, R. Sachs, Y. Barlas, and J. Shi, “Proximity-induced ferromagnetism in graphene revealed by the anomalous Hall effect,” *Phys. Rev. Lett.* **114**, 016603 (2015).
- [30] A. G. Swartz, P. M. Odenthal, Y. Hao, R. S. Ruoff, and R. K. Kawakami, “Integration of the ferromagnetic insulator EuO onto graphene,” *ACS Nano* **6**, 10063 (2012).
- [31] S. K. Behera, M. Bora, S. Sindhu, P. Chowdhury, and P. Deb, “Proximity effects in graphene and ferromagnetic CrBr<sub>3</sub> van der Waals heterostructures,” *Phys. Chem. Chem. Phys.* **21**, 25788 (2019).
- [32] K. Takiguchi, L. D. Anh, T. Chiba, T. Koyama,

- D. Chiba, and M. Tanaka, “Giant gate-controlled proximity magnetoresistance in semiconductor-based ferromagnetic–non-magnetic bilayers,” *Nat. Phys.* **15**, 1134 (2019).
- [33] N. Cortés, O. Ávalos-Ovando, L. Rosales, P. A. Orellana, and S. E. Ulloa, “Tunable spin-polarized edge currents in proximitized transition metal dichalcogenides,” *Phys. Rev. Lett.* **122**, 086401 (2019).
- [34] K. Zollner, M. Gmitra, T. Frank, and J. Fabian, “Theory of proximity-induced exchange coupling in graphene on hBN/(Co, Ni),” *Phys. Rev. B* **94**, 155441 (2016).
- [35] G. Giovannetti, P. A. Khomyakov., G. Brocks, V. M. Karpan, J. van den Brink, and P. J. Kelly, “Doping graphene with metal contacts,” *Phys. Rev. Lett.* **101**, 026803 (2008).
- [36] P. U. Asshoff, J. L. Sambricio, A. P. Rooney, S. Slizovskiy, A. Mishchenko, A. M. Rakowski, E. W. Hill, A. K. Geim, S. J. Haigh, and V. I. Fal’ko, “Magnetoresistance of vertical Co-graphene-NiFe junctions controlled by charge transfer and proximity-induced spin splitting in graphene,” *2D Mater.* **4**, 031004 (2017).
- [37] V. M. Karpan, G. Giovannetti, P. A. Khomyakov, M. Talanana, A. A. Starikov, M. Zwierzycki, J. van den Brink, G. Brocks, and P. J. Kelly, “Graphite and graphene as perfect spin filters,” *Phys. Rev. Lett.* **99**, 176602 (2007).
- [38] A. F. Hebard, A. T. Fiory, and R. Eick, “Experimental considerations in the quest for a thin-film superconducting field-effect transistor,” *IEEE Trans. Magn.* **23**, 1279 (1987).
- [39] J. Mannhart, J. Ströbel, J. G. Bednorz, and C. Gerber, “Large electric field effects in  $\text{YBa}_2\text{Cu}_3\text{O}_{7-d}$  films containing weak links,” *Appl. Phys. Lett.* **63**, 630 (1993).
- [40] J. Xu, S. Singh, J. Katoch, G. Wu, T. Zhu, I. Žutić, and R. K. Kawakami, “Spin inversion in graphene spin valves by gate-tunable magnetic proximity effect at one-dimensional contacts,” *Nat. Commun* **9**, 2869 (2018).
- [41] A. Kokalj, “XCrySDen — a new program for displaying crystalline structures and electron densities,” *J. Mol. Graph. Model* **17**, 176 (1999).
- [42] J. J. Mortensen, L. B. Hansen, and K. W. Jacobsen, “Real-space grid implementation of the projector augmented wave method,” *Phys. Rev. B* **71**, 035109 (2005).
- [43] J. Enkovaara, C. Rostgaard, J. J. Mortensen, J. Chen, M. Dułak, L. Ferrighi, J. Gavnholt, C. Glinsvad, V. Haikola, H. A. Hansen, H. H. Kristoffersen, M. Kuisma, A. H. Larsen, L. Lehtovaara, M. Ljungberg, O. Lopez-Acevedo, P. G. Moses, J. Ojanen, T. Olsen, V. Petzold, N. A. Romero, J. Stausholm-Møller, M. Strange, G. A. Tritsarlis, M. Vanin, M. Walter, B. Hammer, H. Häkkinen, G. K. H. Madsen, R. M. Nieminen, J. K. Nørskov, M. Puska, T. T. Rantala, J. Schiøtz, K. S. Thygesen, and K. W. Jacobsen, “Electronic structure calculations with GPAW: a real-space implementation of the projector augmented-wave method,” *J. Phys.: Condens. Matter* **22**, 253202 (2010).
- [44] A. H. Larsen, J. J. Mortensen, J. Blomqvist, I. E. Castelli, R. Christensen, M. Dułak, J. Friis, M. N. Groves, B. Hammer, C. Hargus, E. D. Hermes, P. C. Jennings, P. B. Jensen, J. Kermode, J. R. Kitchin, E. L. Kolsbjerg, J. Kubal, K. Kaasbjerg, S. Lysgaard, J. B. Maronsson, T. Maxson, T. Olsen, L. Pastewka, A. Peterson, C. Rostgaard, J. Schiøtz, O. Schütt, M. Strange, K. S. Thygesen, T. Vegge, L. Vilhelmsen, M. Walter, Z. Zeng, and K. W. Jacobsen, “The atomic simulation environment—a Python library for working with atoms,” *J. Phys.: Condens. Matter* **29**, 273002 (2017).
- [45] V. O. Ö. H. Hakan Gürel and S. Cirac, “Effects of charging and perpendicular electric field on the properties of silicene and germanene,” *J. Phys.: Condens. Matter* **22**, 253202 (2013).
- [46] K. Berland and P. Hyldgaard, “Exchange functional that tests the robustness of the plasmon description of the van der Waals density functional,” *Phys. Rev. B* **89**, 035412 (2014).
- [47] K. Berland, C. A. Arter, V. R. Cooper, K. Lee, B. I. Lundqvist, E. Schröder, T. Thonhauser, and P. Hyldgaard, “van der Waals density functionals built upon the electron-gas tradition: Facing the challenge of competing interactions,” *J. Chem. Phys.* **140**, 18A539 (2014).
- [48] F. Tran, L. Kalantari, B. Traoré, X. Rocquefelte, and P. Blaha, “Nonlocal van der Waals functionals for solids: Choosing an appropriate one,” *Phys. Rev. Materials* **3**, 063602 (2019).
- [49] A. H. Larsen, M. Kuisma, J. Löfgren, Y. Pouillon, P. Erhart, and P. Hyldgaard, “libvdwxc: a library for exchange–correlation functionals in the vdW-DF family,” *Modelling Simul. Mater. Sci. Eng.* **25**, 065004 (2017).
- [50] P. E. Blöchl, “Projector augmented-wave method,” *Phys. Rev. B* **50**, 17953 (1994).
- [51] P. E. Blöchl, C. J. Först, and J. Schimpl, “Projector augmented wave method: ab initio molecular dynamics with full wave functions,” *Bull. Mater. Sci.* **26**, 33 (2003).
- [52] J. P. Perdew, K. Burke, and M. Ernzerhof, “Generalized gradient approximation made simple,” *Phys. Rev. Lett.* **77**, 3865 (1996).
- [53] D. Stradi, L. Jelier, S. Smidstrup, and K. Stokbro, “Method for determining optimal supercell representation of interfaces,” *J. Phys.: Condens. Matter* **29**, 185901 (2017).
- [54] J. Tersoff and D. R. Hamann, “Theory of the scanning tunneling microscope,” *Phys. Rev. B* **31**, 805 (1985).
- [55] E. Y. Tsybal and I. Žutić (editors), *Spintronics Handbook Spin Transport and Magnetism, 2nd Edition* (Taylor & Francis/CRC Press, Boca Raton, FL, 2019).
- [56] H. Dery, Y. Song, P. Li, and I. Žutić, “Silicon spin communications,” *Appl. Phys. Lett.* **99**, 121111 (2011).
- [57] T. C. Zhu, S. Singh, J. Katoch, H. Wen, K. Belashchenko, I. Žutić, and R. K. Kawakami, “Probing tunneling spin injection into graphene via bias dependence,” *Phys. Rev. B* **98**, 054412 (2018).
- [58] M. Gurram, S. Omar, and B. van Wees, “Bias induced up to 100% spin-injection and detection polarizations in ferromagnet/bilayer-hBN/graphene/hBN heterostructures,” *Nat. Commun.* **8**, 248 (2017).